PNAS

Size matters: An asymmetry in wave scaling drives outsized quantities of coastal wetland erosion

Rusty A. Feagin[1,2,3] *, Kuang-An Chang[3,4], Thomas P. Huff[2] , Ignacio Rodriguez-Iturbe[3] , Jin-Young Kim[3,4] , James Kaihatu[3,4] , Nicoletta Leonardi[5] , Sergio Fagherazzi[6]

[1]School of Geography and the Environment, University of Oxford, UK
[2]Dept. Ecology and Conservation Biology, Texas A&M University, College Station, TX USA
[3]Dept. Ocean Engineering, Texas A&M University, College Station, TX, USA
[4]Dept. Civil and Environmental Engineering, Texas A&M University, College Station, TX, USA
[5]Dept. Geography and Planning, University of Liverpool, UK
[6]Dept. Earth and Environment, Boston University, MA, USA
*Corresponding Author.

Email: cenv0936@ox.ac.uk; feaginr@tamu.edu

Author Contributions: RAF, K-AC, JK designed the study and wrote and edited text. RAF, TPH, J-YK, NL analyzed data and wrote and edited text. IR-I and SF wrote and edited text.

Competing Interest Statement: The authors have no competing interests.

Classification: Physical Sciences, Environmental Sciences

Keywords: wave erosion, salt marsh, wetlands

This PDF file includes:

Main Text
Figures 1 to 3
Supporting Information

Abstract

Wetlands around the world are susceptible to wave erosion. Analytical work has suggested that the lateral erosion on their edges should be linearly related to the wave power, but several field studies have shown a wide range of variability across site locations. Non-wave factors at these sites, such as variable soil properties and gravity-induced slumping, have confounded the discovery of a more universal relationship. After isolating the effect of these complicating factors using new theory, laboratory, and field datasets, we discovered a key asymmetric scaling relationship between lateral erosion and the individual components of wave power. Surprisingly, lateral erosion rates accelerate non-linearly as waves increase in height, but decelerate non-linearly as waves become longer in length. These findings suggest that wetlands and other sheltered coastlines likely experience outsized quantities of erosion, as compared to oceanic-facing coastlines.

Significance Statement

We discovered that a key asymmetric relationship in wave scaling drives outsized quantities of lateral wetland erosion.

Main Text

Introduction

Waves erode wetland shorelines in a wide variety of locations around the world [1]. An important and open question is whether the lateral erosion of their edges, or E, can be predicted as a function of the intercepting waves. As a first guess, early work [2] posited that the energy and erosive shear stress generated by a single wave traveling through deep water should be roughly proportional to the square of its wave height, or H^2 (note: a list of variables can be found after the *Materials and Methods* section). Taking this line of thinking a step further, analytical [3] and numerical [4] work has suggested that the lateral erosion of a vertical wetland edge is linearly related to the wave power, or a combination of H^2 and the wave period T where $E \propto (H^2 T)^x$ with x = 1.

In contrast however, a wide range of field-based studies have identified a non-linear fit between lateral erosion and wave power, with x = 1.10 to 1.37, e.g. [5-10]. These studies have shown a large amount of variability in erosion across field sites, caused by differences in soil properties, vegetation, and myriad other factors [11]. While these inherent differences among the sites can be partially accounted for through mean-standardization [12], non-wave effects still contaminate the field datasets and raise the exponent x. For example, mass wasting [13], tidal creek flows [14-15], alongshore current velocity-driven erosion [11, 16], precipitation driven-erosion [17], and soil cracking due to wetting and drying effects [18] each occur at different frequencies across time [19-23]. A

longer duration field study generally will have (a) more of these non-wave effects embedded within the reported measurements, and (b) a higher average wave power as the likelihood of encountering large wave events increases over time – with the net effect raising the exponent. These non-wave effects also occur in variable quantities depending on each unique study, which further induces scatter into the non-linear fit, particularly as the wave power increases [11]. Both inherent site variation and these non-wave effects have complicated the discovery of a more universal relationship between lateral erosion and wave mechanics.

Our overall objective was to identify the relationship between lateral erosion and several key wave parameters, after isolating these extraneous effects. To do so, we first collected several empirical datasets in the laboratory to explore the relationship between lateral erosion at the shoreward position of a vertical edge of wetland, E, and wave height H, wavelength L, and water depth h_* (see *Materials and Methods* section below). Our laboratory datasets are the first among the literature to isolate the unique effect of each of these parameters to wetland edge erosion, including the variability in the vertical dimension. From among many convolutions of the variables, we then found the best fit with E and sought to describe the physics of the wave-conversion-to-erosion process from a first principles perspective.

In this same laboratory dataset, we next explored the statistical properties of the individual lateral erosional depths, or "chunks" with a depth of e, that occurred across the vertical face of the eroding edge and related them back to E. We then collected lateral erosion data from across three continents at field sites with a variety of H, L, and h_* conditions, as documented further in [12]. We mean-standardized the left and right sides of Eq. 1 by site location which converted them into what [12] refers to as E^* and P^*, respectively, and inserted the laboratory data (see *Materials and Methods* below). Our results led us towards a new theoretical conception of how waves induce lateral erosion.

Results

Edge Erosion in the Laboratory

With our laboratory work, we first found that lateral erosion E was a non-linear function of wave power as one might expect when holding all other variables constant, similar to the aforementioned field studies, though with a far lower exponent of x = 0.65 (See Supporting Information, SI Figs. S1-2). We attribute this lower value to the removal of the non-wave effects.

However, we found that the best fit was more complex and included a permutation of multiple variables (Fig. 1a). While increasing the wave height H generally increased the cross-shore orbital velocities u in the water column, the water depth at the immediate

edge h_* also affected them by altering the breaking wave form and thus the vertical breadth, location, and magnitude of erosion (SI Figs. 3-4). The best statistical fit for the data included the wave height, steepness, and the breaking form effects as:

$$E \propto \left(H^2 \times \sqrt{\frac{H}{L}} \times \frac{L}{h_*} \right)^{\zeta} \quad \text{Eq. 1}$$

In this formulation, the lateral erosion was proportional to the product of the wave energy, the square root of the wave steepness, and the inverse of the relative water depth (which accounted for breaking form effects). Both sides of the equation could also be divided by time duration t to obtain a lateral erosion rate (as depicted in Fig. 1a). The scaling exponent ζ described the transformation from two-dimensional wave geometry into one-dimensional lateral erosion (see Supplementary Information *Derivations and Dimensionality of Equations*).

For this same laboratory data, E was in fact the mean of a large number of individual lateral erosional depths, e, that occurred across the vertical face of the eroding edge (Fig. S5). We found that the spatial frequency f of encountering these e was inversely proportional to their magnitude, over a wide range of spatial scales (Fig. 2).

Relatively larger e depths were fewer in number, and this limitation exhibited reasonably consistent power law behavior over a range of frequency scales where $e = 1/f^{0.25}$. This range for e was bounded on its lower magnitude end by the mean of the distribution, which was equivalent to E (Figs. S6-7). The distribution was long-tailed and positively skewed towards larger e. One potential explanation for this distribution was that the dynamics of the mechanical erosion process were dampened, with negative feedback limiting the number of the deeply eroding chunks of material. This behavior consistently scaled across all H.

Edge Erosion in the Field

We found nearly the same statistical fit across the field sites for E^* (Fig. 1b) as we had found for the laboratory data for E, suggesting that Eq. 1 provided at least a first-order approximation of the relevant dynamics across the sampled field locations. Indeed, the field data showed greater scatter and a lower r-square than the laboratory data, as expected from data distributed across many site locations around the globe. Yet because E^* had been standardized by site location, the remaining variance was less likely to be due to differences in soil erodibility caused by soil properties or vegetation. Rather, this variance was more likely due to non-wave processes such as mass wasting and slumping which acted differentially over the unique time lengths for which each data point had been collected, or a complex combination of these factors.

To further highlight this concept, we converted Eq. 1 into units of work that accounted for cross-site variations in soil erodibility. For consistent units of measurement in the equation, we first squared both sides, and then on the right-hand side inserted the

common terms for wave energy density $\frac{1}{8}\rho g H^2$ in place of H^2, and the shallow water wave period $T\sqrt{gh}$ in place of L (or alternately, the deepwater wave period $\frac{g}{2\pi}T^2$, see SI-*Derivations and Dimensionality of Equations*). On the left-hand side, we added the bulk density of the sediment φ, and gravitational acceleration g of its movement. We then redistributed and separated out the constant terms, yielding:

$$E^2 \varphi g \;=\; H^{2.5} \times T^{0.5} \times \frac{\rho g^{1.25}}{8 h_*^{0.75}} \qquad \text{Eq. 2}$$

where both sides were made into units of work (kilograms meters^2 seconds^{-2}) through selective cancelation, or otherwise dimensionless through stacking (see SI-*Derivations and Dimensionality of Equations*).

Thus, based on the bulk density, other sediment or site erosion characteristics (in particular φ on the left hand side of Eq. 2), the data points in Fig. 1a could be shifted vertically along the y axis, while the relative slope of the regression line remained the same, as a function of the wave conditions (right hand side); this was the reason behind the common slope across site location in Fig. 1b, upon mean-standardization. In other words, site locations with different soil erodibility had different absolute erosion quantities, but the relative scaling of the lateral erosion as a function of the wave conditions was constant across sites.

Discussion

Asymmetry between Wave Power and Edge Erosion

The laboratory data is the first among the literature to isolate the contribution of H, L, and h_* to lateral erosion, in an empirical manner and with variability in the vertical dimension. Although there have been many past studies that have investigated the effects of waves on wetland erosion, these studies were conducted over longer time periods in the field and thus their measured erosion rates also reflected the influence of non-wave erosion processes. In the existing lab studies that did exist, e.g. [18], the purpose was in fact to induce these non-wave processes. We controlled the laboratory conditions to exclusively investigate the continuous impact of waves alone.

Using this clean laboratory dataset, an asymmetric relationship between lateral erosion and the two components of wave power, H and T, emerged from Eqs. 1-2 when using shallow water formula and removing the constants and depth as:

$$E \propto H^{1.25} T^{0.25} \qquad \text{Eq. 3}$$

or alternately as $E \propto (H^{2.5}T^{0.5})^{\zeta}$ with $\zeta = 0.5$. Eq. 3 provides the best and most simple fit for the controlled, wave-only conditions (Figs. S1-2).

As the exponents in Eq. 3 explicitly describe, lateral erosion is more efficient when the wave power is packed into the wave height as opposed to length. In other words, lateral erosion rates non-linearly accelerate as waves increase in height, but non-linearly decelerate as waves become longer in length.

Eroding Surface Geometry as a Mechanism for the Asymmetry

We can potentially explain the mechanism that caused the asymmetry by generating a hypothesis about the geometry of the individual erosion depths e relative to the wave height H. The following description used our knowledge of the empirical $1/f^{0.25}$ distribution of the e erosional depths, but it also greatly simplified the relevant processes by assuming that the waves were sinusoidal and that their relative water velocities were distributed by distance to the mean water line (see SI-*Expanded Discussion)*. An expansion to non-linear waves would be straight-forward mathematically (it would only slightly alter the relations, while achieving the same general effect as our wave steepness parameter in Eq. 1), but much more difficult to denote and conceptualize. However, we needed only a first order description to identify the relevant geometry at play.

First, we set a generalized vertical dimension h to record all possible water levels that intercepted the edge during a H wave and recorded them as distances h_y from the mean water depth h_* (Fig. 3a). The maximum and minimum of this wave reached $h_{\pm y-limit}$ on either side of h_*, which then set the wave height along this dimension as $H = 2(h_{\pm y-limit})$. With no alongshore variation in the lab waves, we assumed that the variation in e was due to this vertical dimension alone, and that the erosion was greatest at h_*. Using the known frequency distribution (Fig. 2), we accordingly made each e proportional to its vertical distance from h_* in the y direction (Fig. 3b), writing this as $e_y \propto (1/h_y)^{0.25}$.

Next, we built a relation between the one-dimensional (horizontal erosional depth) measure of E and the sum of all one-dimensional e_y erosion depths across h_y, as $E \propto 2\int_{h_*}^{h_{\pm y-limit}} e_y(h_y)$ and thus $E \propto 2\int_{h_*}^{h_{\pm y-limit}} (1/h_y)^{0.25}\,(h_y)$. Its right-hand side then became $2(h_{\pm y-limit})^{1.25}$ after integrating e across all h_y. With substitution of H for $2(h_{\pm y-limit})$ as described in the paragraph above, the erosion rate then scaled as $E \propto H^{1.25}$. This rate was equivalent to $E \propto (H^{2.5})^{\zeta}$ with ζ = 0.5, as one could find from the wave height terms alone in Eqs. 1 and 3.

The $e_y \propto (1/h_y)^{0.25}$ proportionality occurred within a domain of the h_y dimension that stretched from the largest e located at the central portion of the edge at h_*, out to the mean e. For e smaller than the mean (out towards the upper and lower portion of the eroding edge), we wrote $e_y \propto (1/h_y)^1$ because the proportionality scaled linearly in this second domain, empirically (Figs. S8-9). The additive result of the two domains for

the entire distribution was trivial as the inner domain ultimately drove the asymmetric scaling relation of $E \propto H^{1.25}$.

The result of $E \propto H^{1.25}$ was that as waves increase in height alone, their ability to cause erosion became increasingly more efficient due to the geometry of the eroding surface. The erosion rate not only increased, it accelerated non-linearly as wave heights became larger. The laboratory data and the statistical geometry of e depths exhibited this scaling relationship empirically, and our hypothesis provided a potential mechanistic explanation.

Within our datasets, the steep erosional pockets composed of e depths became increasingly deep at an exponential rate in statistical terms. We suggest that a wave's penetration efficiency into these pockets was likely limited by negative feedback with the internal angle of the eroding surface, and an increase in wave height better exploited the geometry of the total edge by biasing more of its energy to areas outside of these pockets. Importantly however, we note that the spatial patterning was somewhat more heterogeneous across h than in our hypothesis, though it still appears to be a statistically valid explanation (eg, Fig 3b versus Fig. S4). Conversely, an increase in the wavelength likely put the wave energy into the horizontal dimension, which was more easily reduced by these pockets through friction induced into the water column (see SI- *Expanded Discussion*). Although we describe the statistical mechanics and their relation to our empirical datasets herein, there will need to be more future work done to address the wave penetration physics in greater detail.

The key inclusion of the wave height-to-wavelength ratio term in Eq. 1 (i.e., $\sqrt{H/L}$), and through conversion into T for Eq. 2 and 3, transformed the wave power into appropriately scaled h versus e erosion terms. Notably, the Iribarren number ξ is known to reduce to $\sqrt{L/H}$ at 45° (ie, [24]) and this fact reinforces the idea that the h versus e erosional shape is likely dependent, but also universally relatable, through the slope of the erosional surface. Once an erosional surface tilts towards a 45° angle, then the erosional height to length process likely equilibrates such that the differential becomes irrelevant, $e_y \propto (1/h_y)^1$, and the erosion will scale linearly with the wave power, as dimensional analysis suggests (ie, $E \propto H^2T$). A dimensional analysis for wetland edges [3] thus could be revised to require symmetry between e and h as a precondition, implying that there is no extra cost to eroding more deeply into narrow spaces, as opposed to the open face of a surface. Once the slope decreases below 45° and towards horizontal, increasing L could become a more efficient mode of increasing erosion (i.e., $E \propto H^{0.25}T^{1.25}$). Differential and asymmetric scaling in erosion should be expected when stretching a wave in only one direction and impacting a non-45° surface, but it has not been considered by previous work on lateral wetland erosion. Further investigations will be required to more fully explore the relevance of this concept across a wide range of coastal slopes.

Effects of the Asymmetry on Coastal Wetland Erosion

Real-world outcomes depend on these fundamentals, regarding the effect of wave heights, lengths, and water depths on wetland erosion. While water waves propagate across more than 73% of the Earth's surface, the relative proximity of the coastline to the location of wave genesis greatly affects the wave height-to-wavelength ratio. In general, the waves that strike wetland edges cross relatively short fetch distances and were created by local wind events. These types of waves are short in wavelength (typically on the order of ~1 cm to 1 m) and steep. In contrast, the waves that strike open ocean shorelines are relatively long in wavelength (~1 m to 10 m), with the wave spectrum having been more strongly organized via wave dispersion. In other words, given the same wave height, a wave generated in a small water body will be more likely to be steeper (due to shorter wavelength).

As a direct consequence of the asymmetry, the erosion rate will be generally higher in smaller water bodies for waves of a given height, with all other parameters being equal. Indeed, wetland edges should be particularly affected by the asymmetry in an out-sized manner, as they are located in relatively sheltered locations.

Similarly, we should also expect that erosion has increased more rapidly on vertical edge surfaces as compared to surfaces less than or equal to 45°, such as on sandy beaches. We can take the concept even a step further, for example given that significant wave heights have increased 7% across coastal portions of the globe from 1986 to 2005 due to wind increases [25]. As a consequence of the non-linear relationship between wave height and erosion, we might expect to find 18% more erosion at the end of this time period. Many new hypotheses, derivative from the asymmetric relationship, can now be tested with existing data, models, and global imagery of shorelines. These erosional outcomes may be surprising, yet we contend that they will be a direct outcome of the asymmetry.

In summary as waves increase in height and impact a vertical surface, the lateral erosion process accelerates in its efficiency – yet simultaneously as waves increase in length, the process decelerates. This seeming contradiction is explained by asymmetric scaling between the individual components of the wave power (wave height versus wavelength) and lateral erosion of a vertical edge. The first principles formulation, the scaling relation, and empirical lab and field results thus point to a new way of conceiving of wetland erosion on vertical edges. The identification and use of a physical description of this process will help scientists, managers and policymakers better mitigate the loss of shorelines around the world.

Materials and Methods

We collected empirical datasets in the laboratory, in the field, and from the literature to explore wave-to-erosion mechanics:

Laboratory. We extracted 0.6 x 0.3 (horizontal footprint) x 0.15 (vertical) m wetland edge samples and then placed them into a 22.9 x 36.6 x 1.2 m wave basin (See SI-Video 1; see [9,26] for more details). We subjected them to a range of regular wave heights (0.01-0.16 m), water depths (0.05-0.26 m), and wave lengths (1.44 m to 3.20 m) common to eroding edges. Water depths were measured relative to the bottom of the samples. Samples were collected from along the immediate edge of a natural marsh in West Galveston Bay, Texas, and prepared using established methods to ensure minimal compaction and a consistent incident surface (e.g., [27]). We recorded the lateral erosion using a Terrestrial Laser Scanner (TLS) LIDAR at 0.5 mm resolution, and then extracted the vegetative roots from the point clouds manually (see [28]). The lateral distance between the before versus after point locations was recorded as an individual erosion depth measurement, e. For each wave height x water depth x wavelength trial, we found the average across all e measurements, and then divided it by the time duration of the trial, to find the lateral erosion E per time t.

Field and Literature. Using data from across three continents, we first graphed dimensionless erosion E^* and dimensionless wave power P^* for the Leonardi et al. (2016) [12] summary dataset. This dataset included site-standardized, original field data collected by [2,5, 29-32]. We added four data points that we collected from a field site in West Galveston Bay, Texas (same location where the laboratory samples had also been collected); this data was collected over 318 days along a 20 m long eroding marsh edge of 0.6 m in height, using the TLS LIDAR and an ultrasonic sensor to measure the wave parameters, as described in [28, 33]. For our laboratory values from Fig. 1a, we first calculated P using the Leonardi et al. (2016) [12] equation ($P = Wc_g$, where $W = \rho g H^2 /8$ and c_g is the group velocity which is equivalent to L/T for the regular lab waves). We then followed their method of mean standardization to find P^* and E^* for each record.

Acknowledgments

Dedicated to the memory of our co-author, Ignacio Rodriguez-Iturbe.

Variables used in equations

E	lateral erosion in the shoreward direction, mean (meters)
H	wave height (meters)
L	wave length (meters)
h_*	water depth, at the erosional edge (meters)
ζ	transfer efficiency (unitless)
t	time duration (seconds)
u	water velocity in the cross-shore dimension (meters per second)
e	lateral erosion of edge, specific to vertical or horizontal position(meters)
f	frequency of occurrence for e (count)
$h, h_y, h_{\pm y-limit}$	vertical dimension of eroding edge, distance from h_* on y axis (meters)
k	wavenumber (per meter)
ω	angular frequency (per second)
E^*	lateral erosion, standardized by mean E from across-site data (unitless)
P^*	lateral erosion, standardized by mean P from across-site data (unitless)
T	wave period (seconds)
ρ	water density (kilograms per meter)
g	gravitational acceleration (meters per second^2)
φ	sediment density (kilograms per meter^3)
ξ	Iribarren number (unitless)

References

(1) Kirezci, E., Young, I.R., Ranasinghe, R., Muis, S., Nicholls, R.J., Lincke, D., Hinkel, J. Projections of global-scale extreme sea levels and resulting episodic coastal flooding over the 21st Century. *Scientific Reports* **10**: 11629 (2020).

(2) Dean, R.G., Dalrymple, R.A. Water Wave Mechanics for Engineers and Scientists. World Scientific Publishing, Singapore (1991), 368 pp.

(3) Marani, M., D'Alpaos, A., Lanzoni, S., Santalucia, M. Understanding and predicting wave erosion of marsh edges. *Geophysical Research Letters* **38**: L21401.(2011).

(4) Tommasini, L., Carniello, L., Ghinassi, M., Roner, M., D'Alpaos, A. Changes in the wind-wave field and related salt-marsh lateral erosion: Inferences from the evolution of the Venice Lagoon in the last four centuries. *Earth Surface Processes and Landforms*: **44** 1633-1646. (2019).

(5) Schwimmer, R.A. Rates and processes of marsh shoreline erosion in Rehoboth Bay, Delaware, U.S.A. *Journal of Coastal Research* **3**, 672-683. (2001).

(6) Karimpour, A., Chen, Q., Twilley, R.R. A field study of how wind waves and currents may contribute to the deterioration of saltmarsh fringe. *Estuaries and Coasts* **39**: 935-950. (2016).

(7) Ortiz, A.C., Roy, S., Edmonds, D.A. Land loss by pond expansion on the Mississippi River Delta Plain. *Geophysical Research Letters* **44**: 3635-3642. (2017).

(8) Valentine, K., Mariotti, G. Wind-driven water level fluctuations drive marsh edge erosion variability in microtidal coastal bays. *Continental Shelf Research* **176**: 76-89. (2019).

(9) Kim, J-Y., Kaihatu, J., Chang, K-A., Sun, S-H., Huff, T., Feagin, R.A. Cold front induced waves acting on the wetlands boundary. *Journal of Geophysical Research: Oceans* **125**: e2020JC016603. (2020).

(10) Bendoni, M., Mel, R., Solari, L., Lanzoni, S., Francalanci, S., Oumeraci, H. Insights into lateral marsh retreat mechanism through localized field measurements. Water Resources Research **52**: 1446-1464. (2016).

(11) Houttuijn Bloemendaal, L.J., FitzGerald, D.M., Hughes, Z.J., Novak, A.B., Georgiou, I.Y. Reevaluating the wave power-salt marsh retreat relationship. *Scientific Reports* **13**: 2884. (2023).

(12) Leonardi, N., Ganju, N.K., Fagherazzi, S. A linear relationship between wave power and erosion determines salt-marsh resilience to violent storms and hurricanes. *Proceedings of the National Academy of Sciences* **113**:64-68. (2016).

(13) Priestas, A.M., Mariotti, G., Leonardi, N., Fagherazzi, S. Coupled wave energy and erosion dynamics along a salt marsh boundary, Hog Island Bay, Virginia, USA. *Journal of Marine Science and Engineering* **3**: 1041-1065. (2015).

(14) Browne, J.P. Long-term erosional trends along channelized salt marsh edges. *Estuaries and Coasts* **40**: 1566-1575. (2017).

(15) Deegan, L.A., Johnson, D.S., Warren, R.S., Peterson, B.J., Fleeger, J.W., Fagherazzi, S. Coastal eutrophication as a driver of salt marsh loss. *Nature* **490**: 388-392. (2012).
(16) Bouma, T.J., de Vries, M.B., Low, E., Kusters, L., Herman, P.M.J., Tanczos, I.C., Temmerman, S., Hesselink, A., Meire, P., van Regenmortel, S. Flow hydrodynamics on a mudflat and in salt marsh vegetation: Identifying general relationships for habitat characterisations. *Hydrobiologia* **540**: 259-274. (2005).
(17) Tolhurst, T.J., Watts, C.W., Vardy, S., Sauders, J.E., Consalvey, M.C., Paterson, D.M. The effects of simulated rain on the erosion threshold and biogeochemical properties of intertidal sediments. *Continental Shelf Research* **28**: 1217-1230. (2008).
(18) Francalanci, S., Bendoni, M., Rinaldi, M., Solari, L. Ecomorphodynamic evolution of salt marshes: Experimental observations of bank retreat processes. *Geomorphology* **195**: 53-65. (2013).
(19) Brooks, H., Moller, I., Carr, S., Chirol, C., Christie, E., Evans, B., Spencer, K.L., Spencer, T., Royse, K. Resistance of salt marsh substrates to near-instantaneous hydrodynamic forcing. *Earth Surface Processes and Landforms* **46**: 67-88. (2020).
(20) van der Wal, D., van Dalen, J., Willemsen, P.W.J.M., Borsje, B.W., Bouma, T.J. Gradual versus episodic lateral saltmarsh cliff erosion: Evidence from Terrestrial Laser Scans (TLS) and Surface Elevation Dynamics (SED) sensors. *Geomorphology* **426**: 108590. (2023).
(21) Wang, H., van der Wal, D., Li, X., van Belzen, J., Herman, P.M.J., Hu, Z., Ge, Z., Zhang, L., Bouma, T.J. Zooming in and out: Scale dependence of extrinsic and intrinsic factors affecting salt marsh erosion. *Journal of Geophysical Research Earth Surface* **122**: 1455-1470. (2017).
(22) van de Koppel, J., van der Wal, D., Bakker, J.P., Herman, P.M. Self-organization and vegetation collapse in salt marsh systems. *American Naturalist* **165**: 1-12. (2005).
(23) Mel, R.A., Bendoni, M., Steffinlongo, D. Salt-marsh retreat on different time scales: Issues and prospects from a 5-year monitoring campaign in the Venice Lagoon. *Earth Surface Processes and Landforms* **47**: 1989-2005. (2022).
(24) Iribarren, C.R., Nogales, C. Protection des ports. Proceedings XVIIth International Navigation Congress, Section II, Communication, 4, Lisbon, (1949), pp. 31-80.
(25) Reguero, B.G., Losada, I.J., Mendez, F.J. A recent increase in global wave power as a consequence of oceanic warming. *Nature Communications* **10**: 205. (2019).
(26) Kim, J-Y. Wetland erosion in Galveston Bay by ocean waves. Ph.D. Thesis (Texas A&M University, College Station). https://hdl.handle.net/1969.1/193212 (2021).
(27) Feagin, R.A., Lozada-Bernard, S.M., Ravens, T., Möller, I., Yeager, K.M., Baird, A.H. Does vegetation prevent wave erosion of salt marsh edges? *Proceedings of the National Academy of Sciences* USA **106**: 10109-10113. (2009).
(28) Huff, T.P., Feagin, R.A., Delgado, Jr., A. Understanding lateral marsh edge erosion with Terrestrial Laser Scanning (TLS). *Remote Sensing* **11**: 2208, 1-12. (2019).

(29) McLoughlin, S., Wiberg, P., Safak, I., McGlathery, K. Rates and forcing of marsh edge erosion in a shallow coastal bay. *Estuaries and Coasts* **38**:620-638. (2014).
(30) Trosclair, K.J. Wave transformation at a saltmarsh edge and resulting marsh edge erosion: Observations and Modeling. PhD thesis (University of New Orleans, New Orleans), (2013).
(31) Tomkins, K., McLachlan, G., Coleman, R. Quantification of coastal bank erosion in Western Port (CSIRO Water for a Healthy Country Flagship, Australia). Water for a Healthy Country Flagship Report Series ISSN: 1835-095X. (2014).
(32) Priestas, A.M. The role of wind waves on salt marsh morphodynamics. PhD thesis (Boston University, Boston), (2013).
(33) Delgado, Jr., A. Quantifying coastal marsh erosion using a LIDAR Terrestrial Laser Scanner: The role of waves, soil, and vegetation. MS Thesis (Texas A&M University, College Station), (2016).

Figures

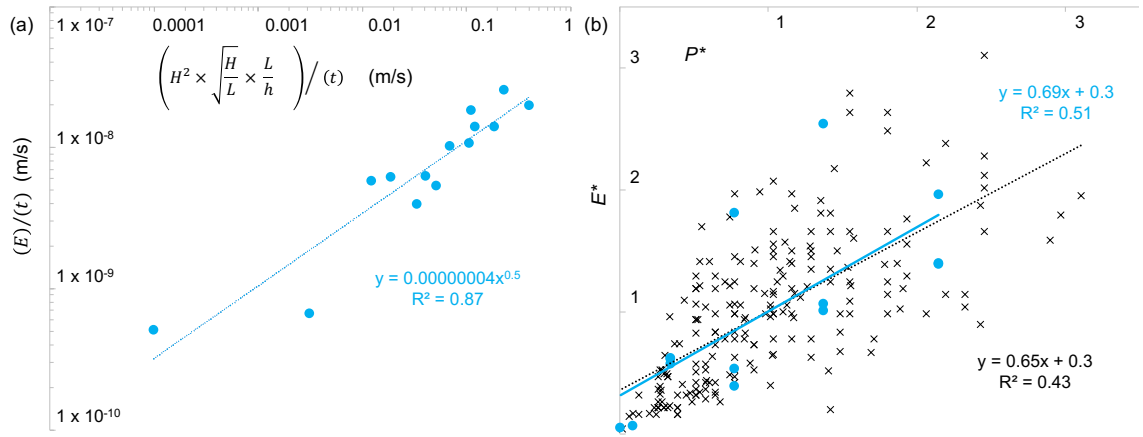

Figure 1. (a) The relation $E \propto \left(H^2 \times \sqrt{\frac{H}{L}} \times \frac{L}{h_*}\right)^{\zeta}$ with ζ = 0.5 provided the best fit for laboratory flume data sets. Dimensionless erosion was obtained by stacking the two sides (in this depiction, the units for both axes were divided by time duration t and thus were in m/s empirically); (b) The laboratory data (blue circles) and field site data from across three continents (black markers) exhibited a similar relationship, when re-graphed as mean-standardized erosion E^* versus wave power P^*. Units for both axes are dimensionless.

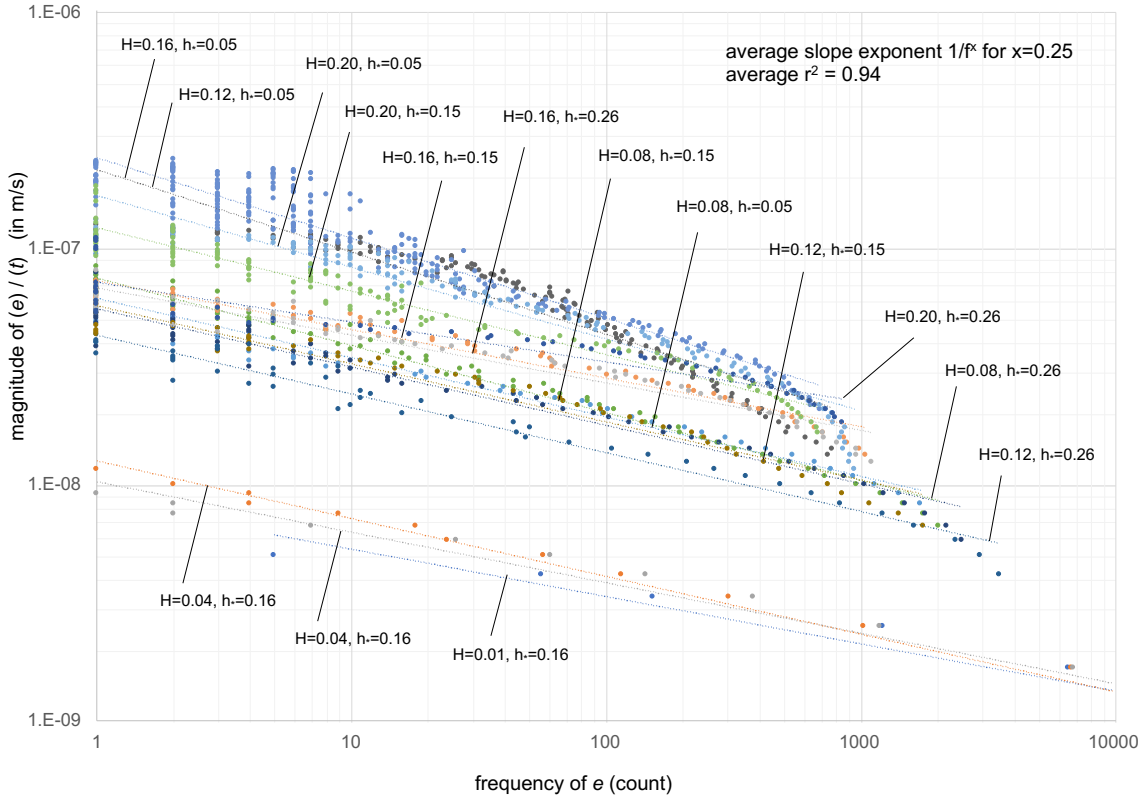

Figure 2. For the laboratory data, the magnitude of individual erosion depths e (on a vertical edge) was inversely related to their frequency of occurrence f, over a wide range of scales. Each dot represents the number of times that a given depth was eroded on the surface of the edge, during the induced H/h_* wave conditions as denoted by the colored linear regression fit lines (depicted here as an erosion rate per time t in m/s, similar to Fig. 1a). The exponential fit for the slope was $e = 1/f^{0.25}$, when averaged across all wave height H/h_* combinations.

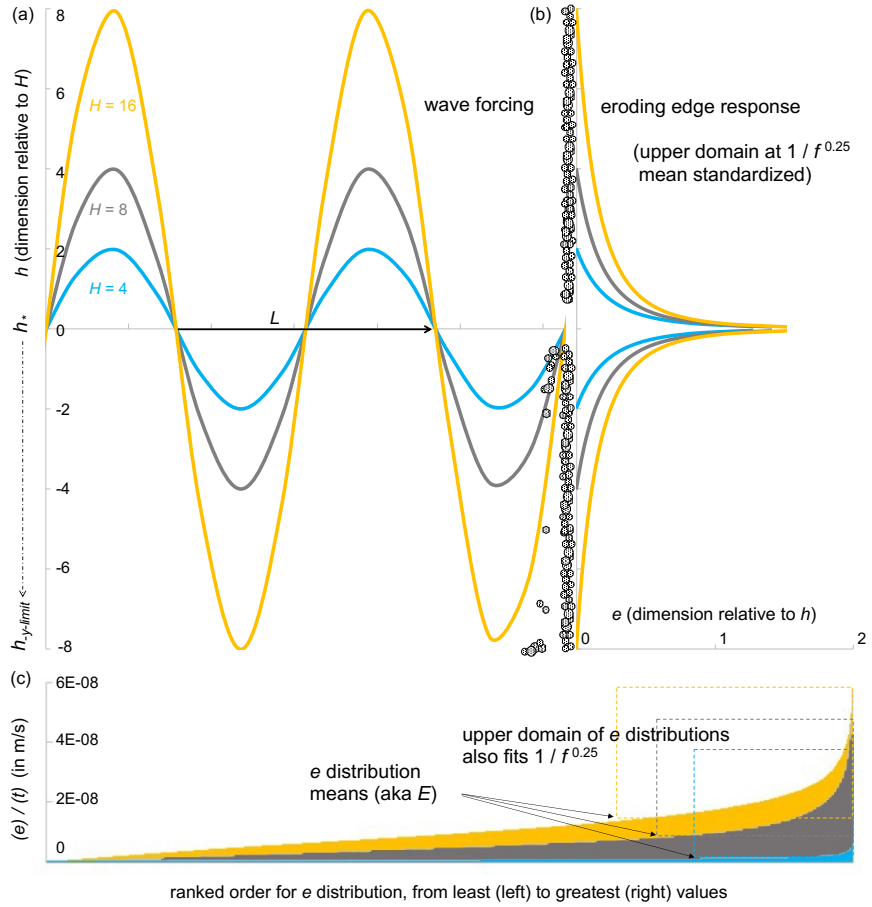

Figure 3. (a) Conceptual depiction of the simplified, mechanistic hypothesis (nonlinear, breaking, and H/h transformed wave forms are not depicted for ease of interpretation of the primary relationship). As waves of varying height H, but constant L, strike a hypothetical edge, (b) their horizontal erosion depths e are proportional to position along a vertical h dimension following a $1/f^{0.25}$ power law. (c) This power law describes the behavior of the upper domain of the e distribution, when it is standardized by the distribution mean, or E. Part (a) and (b) depict the proportional relations only between H, L, and e; they are unitless as depicted. Part (c) depicts empirical lab data ranked in order of e (per time t, in m/s units), using H=16 with h =0.15 (orange), H=8 with h =0.15 (grey), and H =4 with h =0.16 (blue) as examples. The upper domain of these empirical distributions fit the power law (see text, Fig. 2, and SI Figs. S8-9).

Supporting Information for Feagin et al.

Fig. S1. Lateral erosion plotted against the traditional definition of wave power, where the exponent fits as x = 0.65. Only laboratory data is included.

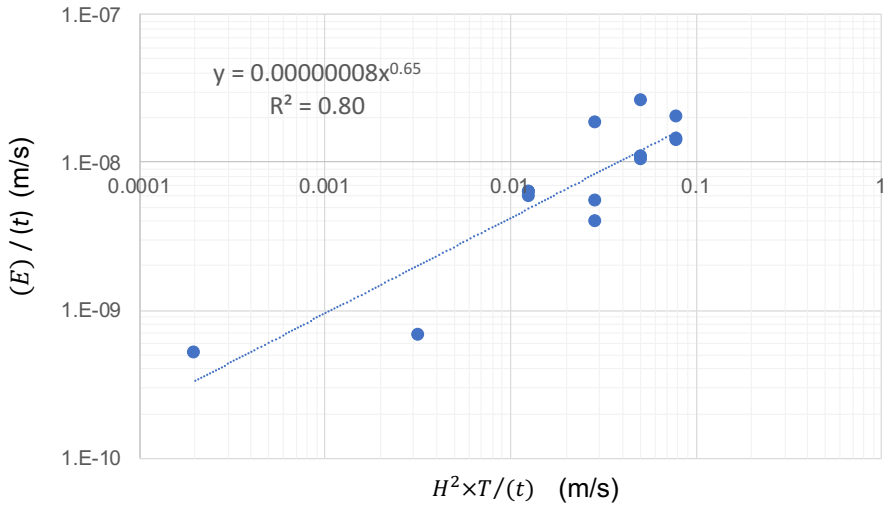

Fig. S2. Lateral erosion plotted against asymmetric wave power, where the exponent fits as x = 1. Only laboratory data is included. The fit is linear with an exponent of 1 – thus the "wave power" scales asymmetrically with respect to lateral erosion as $H^{1.25}T^{0.25}$, when isolating the wave processes and excerpting mass wasting or any other processes. Still, the full version of Eq. 1 has a better r^2 fit and is dimensionless when stacked (as opposed to the simplified Eq. 3 wave power relationship displayed here) – this is because Eq. 1 also includes the relative water depth, and is thus more universal.

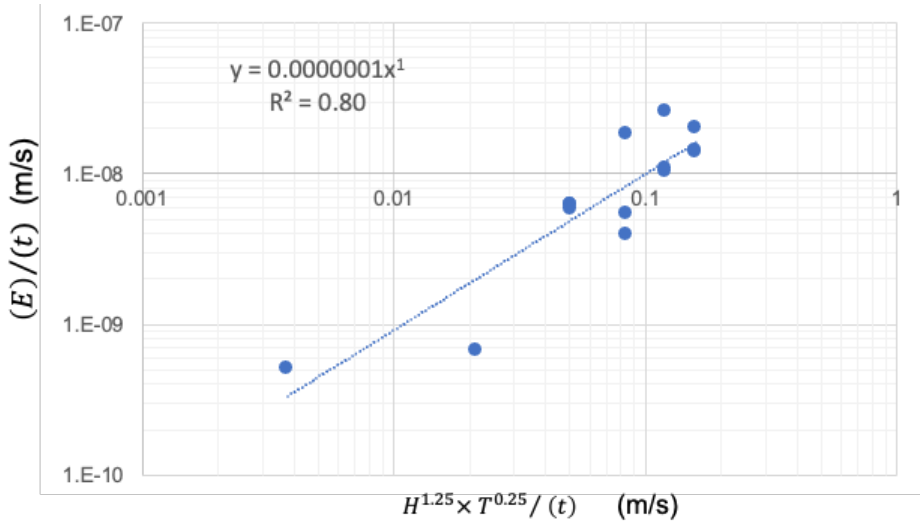

Fig. S3. $H^2 \times \sqrt{\frac{H}{L}} \times \frac{L}{h}$ versus incident water velocity u (m/s), as recorded in the laboratory. Water velocity is in the cross-shore dimension (i.e., intercepting the marsh edge from a horizontal direction). Assuming the fit of $H^2 \times \sqrt{\frac{H}{L}} \times \frac{1}{h}^{\zeta}$ with ζ = 0.5 over a given duration of time, e.g. 1 sec, yields the relationship dimensionless.

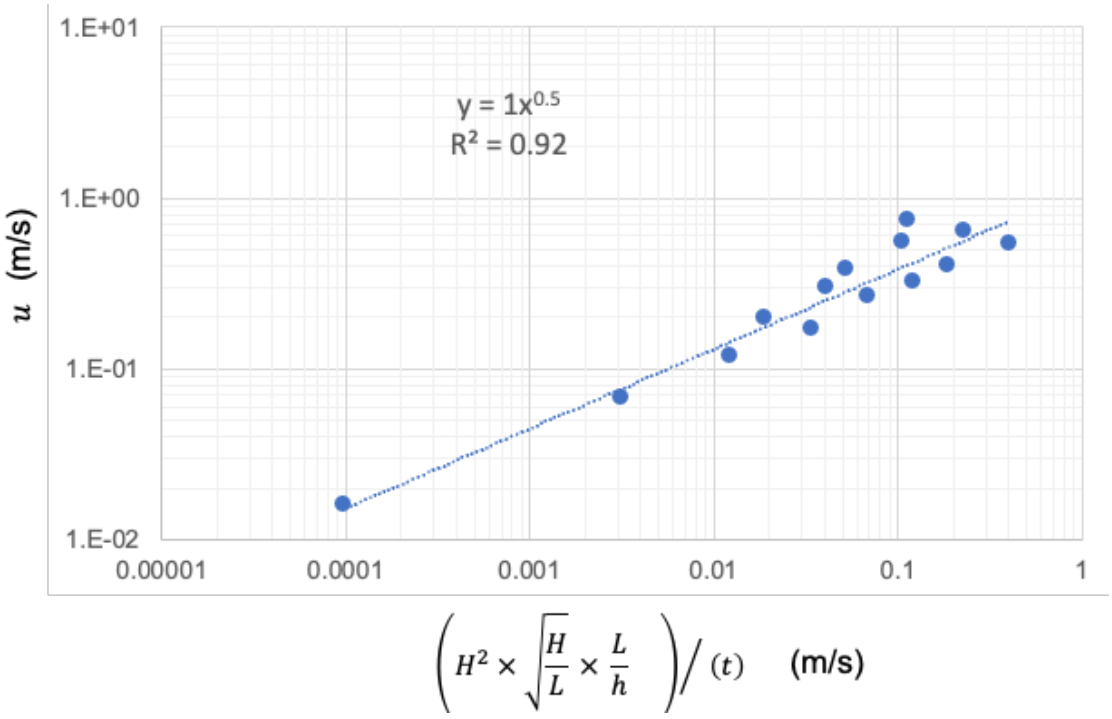

Fig. S4. Erosion depths e varied vertically across the h dimension of the marsh edge, when the still water level h_* was near the top (a), at the mid-point (b), and near the bottom of the edge (c).

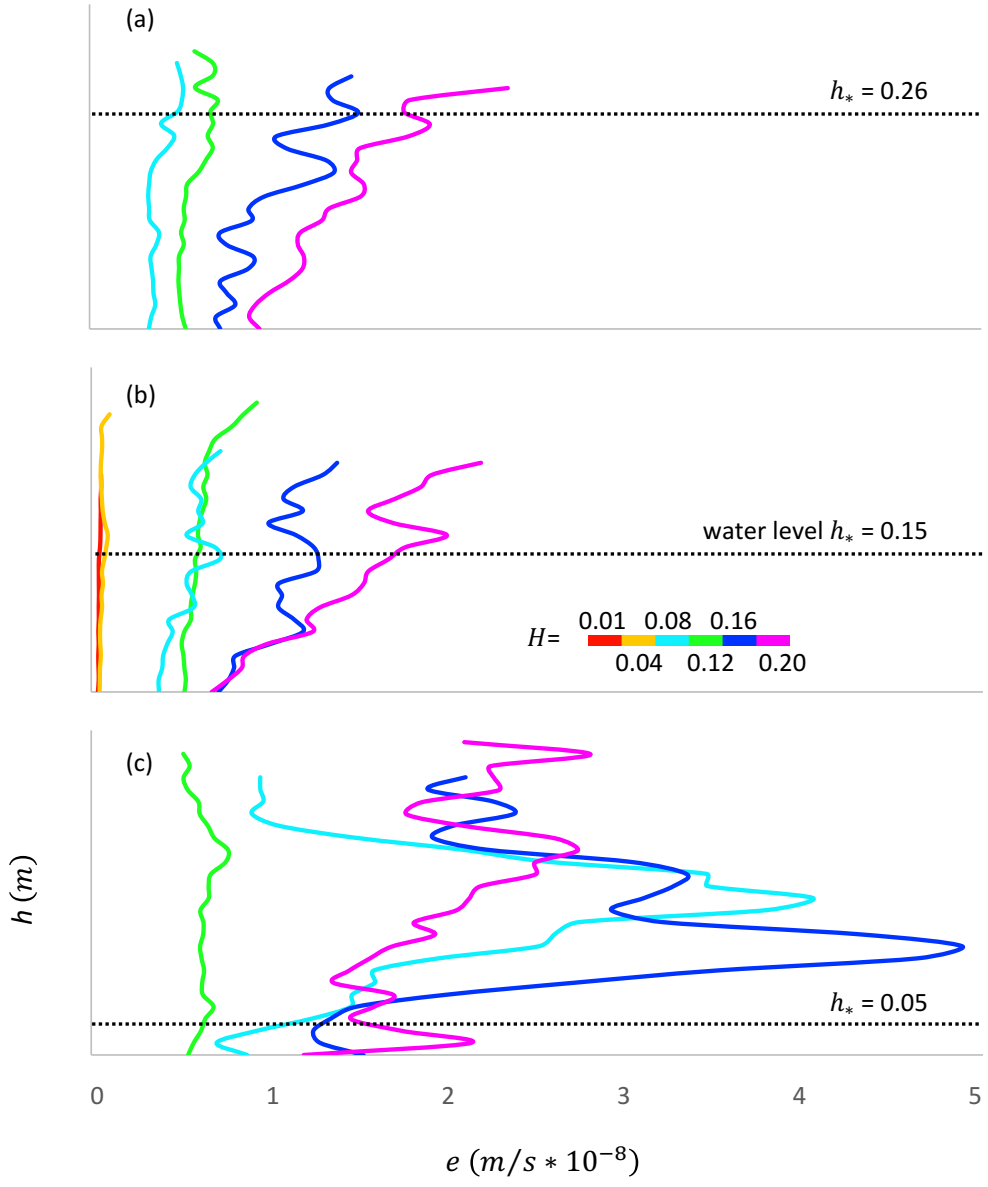

Fig. S5. The cross-sectional area of erosion plotted against the various relations described in the main text (i.e., the sum of e across the vertical dimension h, similar to that depicted in Fig. 3 of the main text). Again, $\zeta = 0.5$ provided the best linear fit.

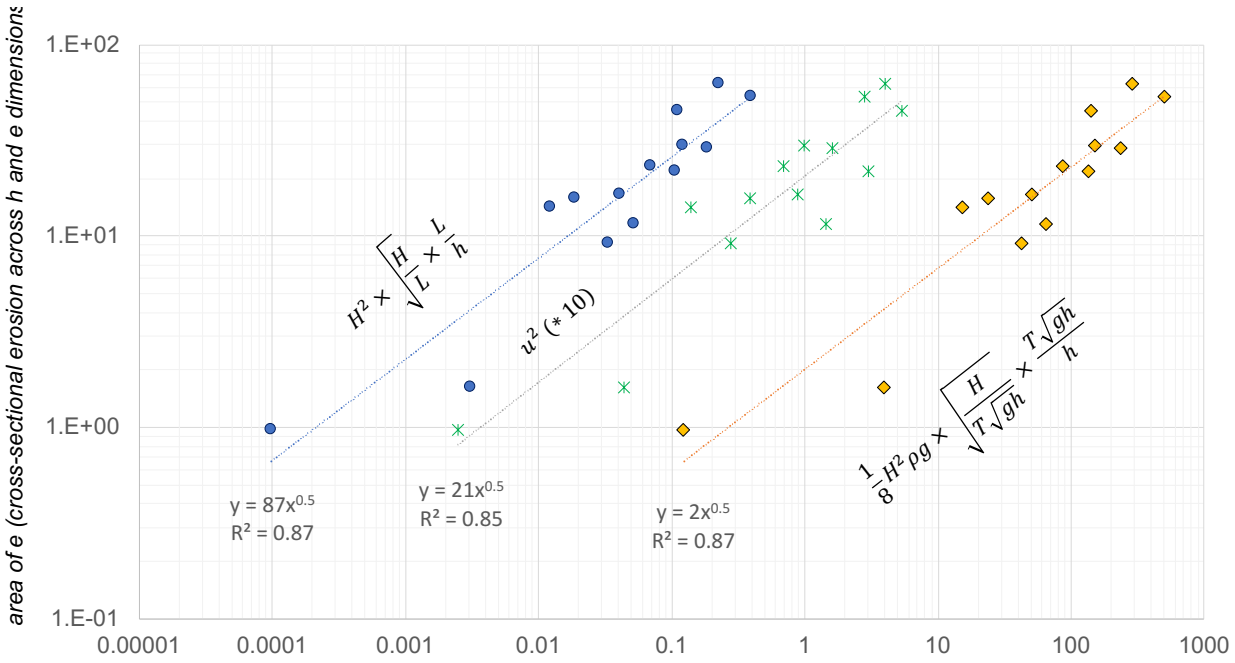

Fig. S6. Full datasets for e frequency distribution (in this graph, the data is not restricted to magnitudes greater than inflection point, i.e. at the mean of distribution, as in Fig. 2 in the main text). For H = 1 and H = 4, the power law extends across the entire domain and the inflection point lay below our detection limits.

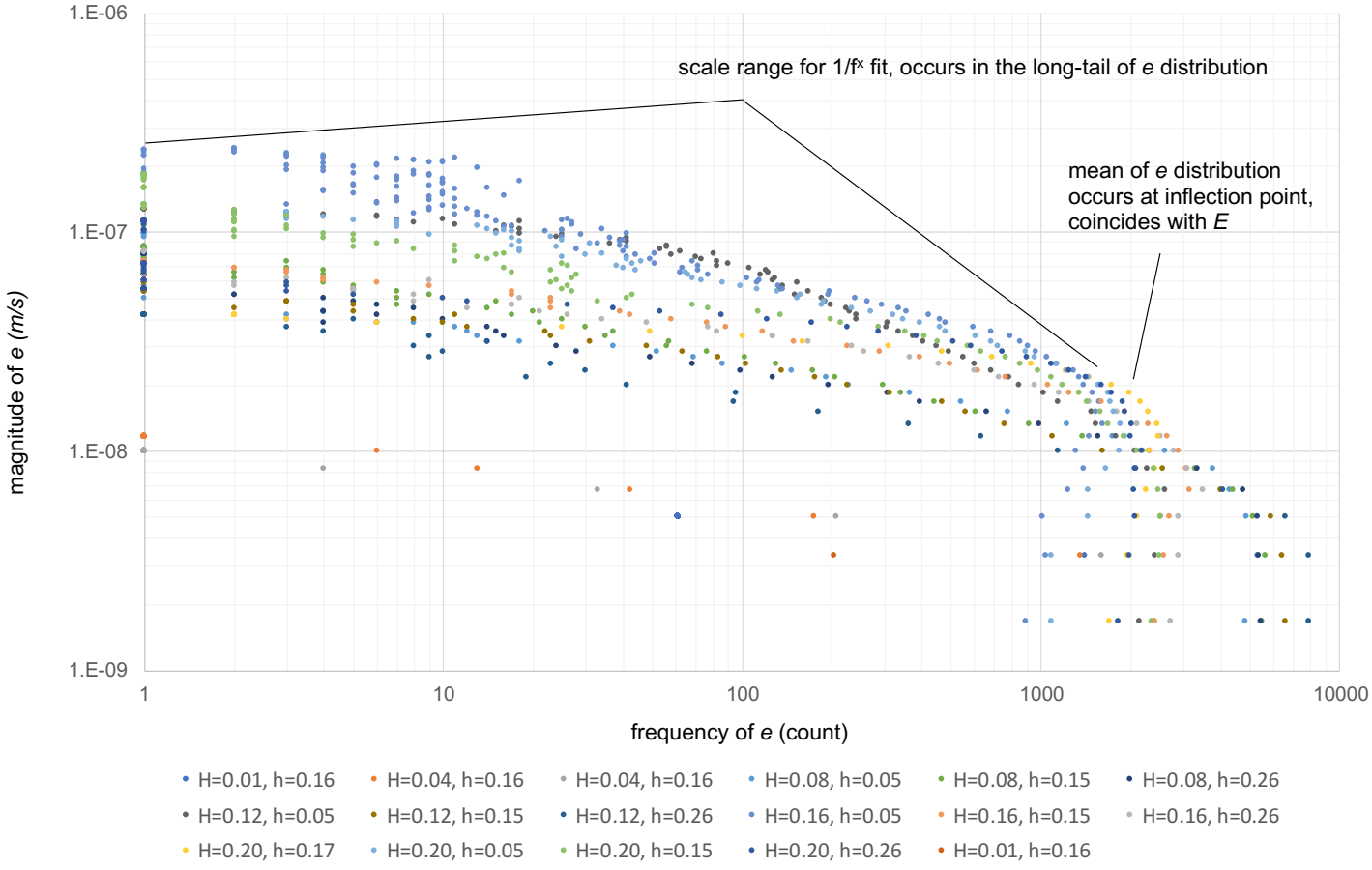

Fig. S7. Datasets for e frequency distributions, grouped by wave height H. Unique exponents and r^2 are shown, for each of the cases that contributed to the averaged $e = 1/f^{0.25}$. The average exponent across all fits was $f = -0.25$. However, each individual fit ranged from -0.11 to -0.34, with the lowest values corresponding to $H = 20$ with $h_* = 0.26$ and the highest to $H = 12$ with $h_* = 0.05$. The slope of the power function fit steepened when H^2/h_* increased. This result highlights the fact that the shape of the e erosion changes in response to wave form. The e distribution is steeper in slope (deeper holes) with plunging waves, and shallower with surging waves. Accordingly, one could solve the $E \propto e * h$ side of Eq. 1 for each of these cases separately, finding that H scales slightly differently in each case; however, for the full Eq. 1, the inclusion of h_* adequately accounts for this variation.

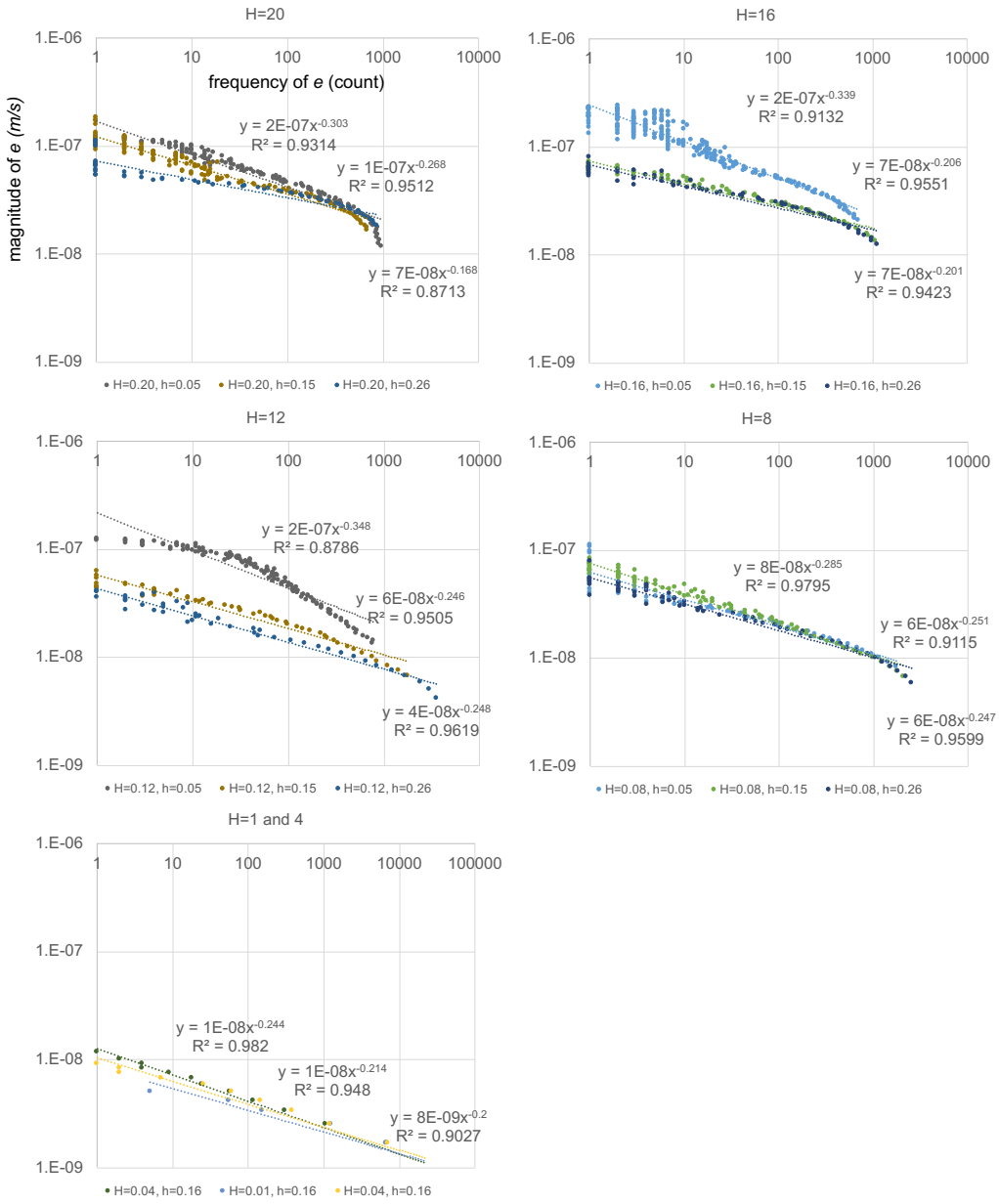

Fig. S8. For *e* individual erosion depths that are greater than the mean value (aka *E*), the distribution generally follows the power law relationship described in the text, across all H/h_* combinations. Values are ranked by magnitude on the x axis.

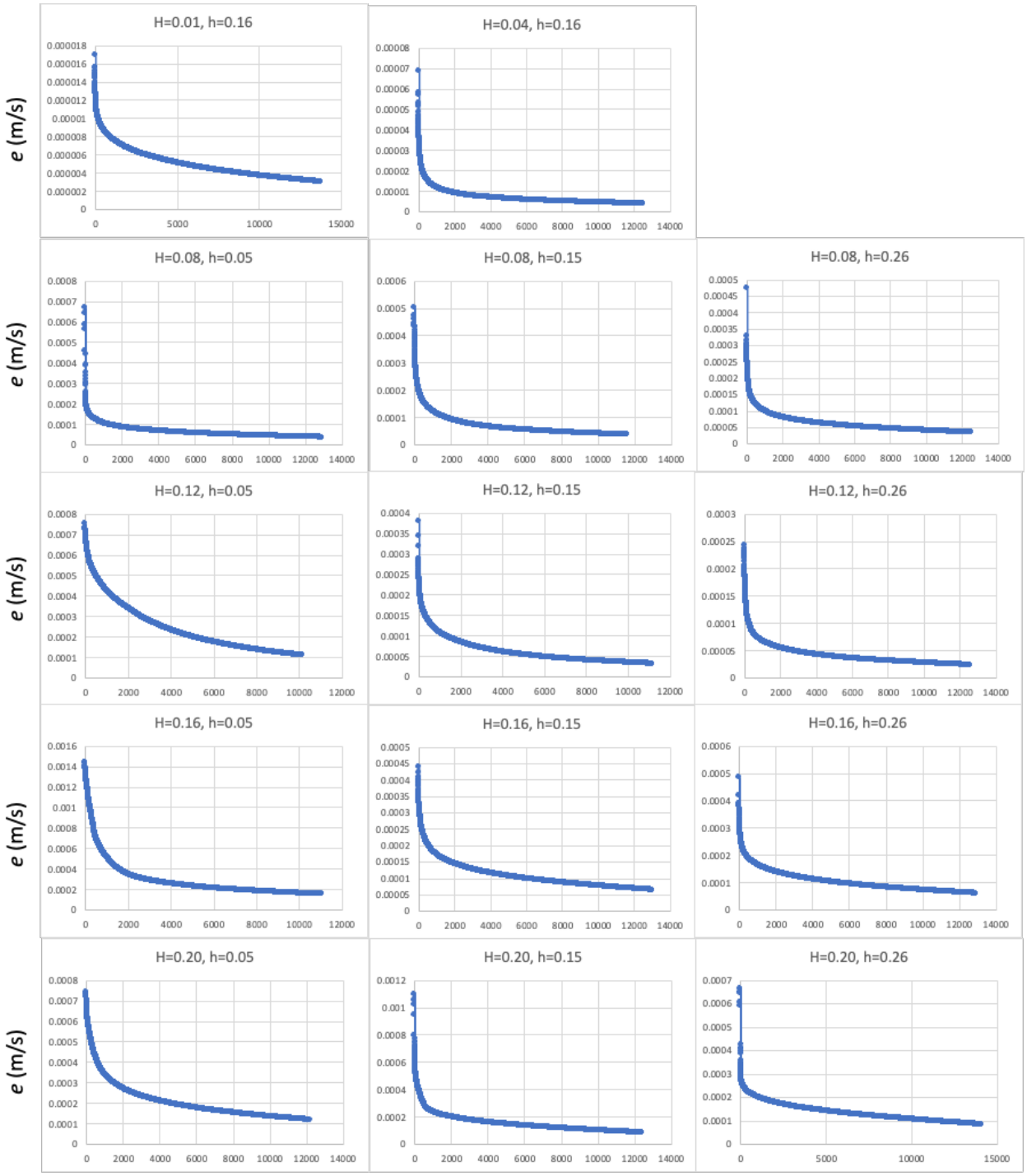

Fig. S9. For *e* individual erosion depths that are less than the mean value (aka *E*), the distribution generally follows the linear relationship described in the text, across all H/h_* combinations. Values are ranked by magnitude on the x axis.

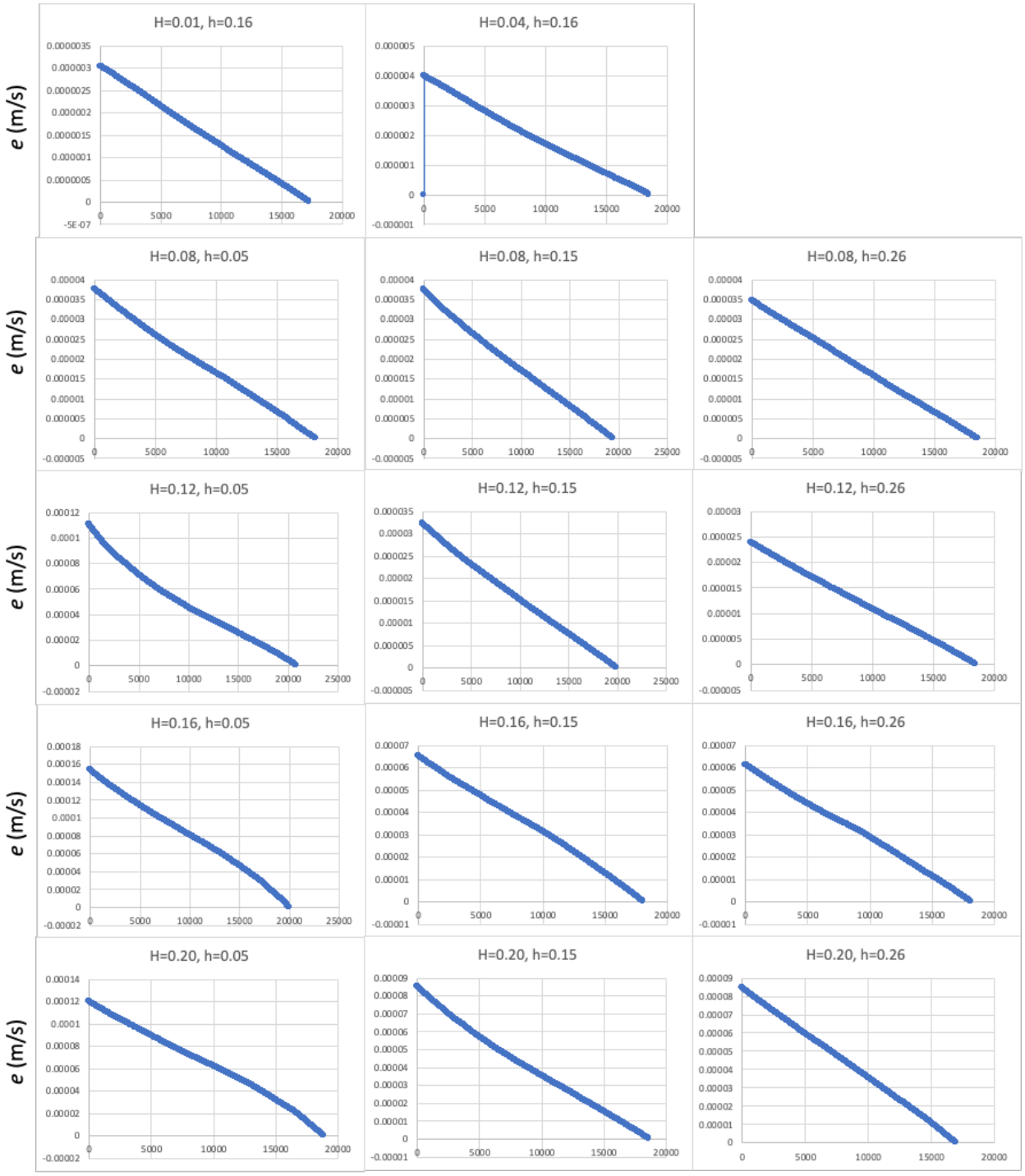

Derivations and Dimensionality of Equations

Dimensionality for Eq. 1

The units cancel out for Eq. 1 from the main text for ζ = 0.5, making the relation dimensionless if stacked:

$$E \propto \left(H^2 \times \sqrt{\frac{H}{L}} \times \frac{L}{h_*} \right)^{\zeta}$$

$$\downarrow$$

$$m \propto \left(m^2 \times \sqrt{\frac{m}{m}} \times \frac{m}{m} \right)^{0.5}$$

$$\downarrow$$

1: 1

OR

$$\frac{E}{\left(H^2 \times \sqrt{\frac{H}{L}} \times \frac{L}{h_*} \right)^{\zeta}}$$

It should be pointed out that for the lab waves (from Fig. 1 in main text), we know that $\zeta = 0.5$. This exponent describes the conversion from a two-dimensional sine wave into a one-dimensional lateral erosion rate E. It also should be pointed out that both sides can also be presented in per-unit time, or the duration over which we allow this wave-to-erosion interaction to occur. So, we could express E as m/s instead of m, and implement the same for the entirety of the right-hand side.

Derivation of Eq. 2, Dimensionality, and Extension to Deepwater

Eq. 2 can be derived from Eq. 1, using ζ = 0.5:

$$E \propto \left(H^2 \times \sqrt{\frac{H}{L}} \times \frac{L}{h_*} \right)^{0.5}$$

To do this, we first square both sides, then we insert the common terms for wave energy density $\frac{1}{8}\rho g H^2$ in place of H^2, and the shallow water wave period $T\sqrt{gh}$ in place of L. Next, to the left hand side, we add the bulk density of the sediment φ, and gravitational acceleration g when it moves:

↓

$$E^2 \varphi g = \frac{1}{8}\rho g H^2 \times \sqrt{\frac{H}{(T\sqrt{gh})}} \times \frac{T\sqrt{gh}}{h_*} \qquad \text{for shallow water}$$

↓

We then offset units and move the terms around to obtain Eq. 2:

$$E^2 \varphi g = H^{2.5} \times T^{0.5} \times \frac{\rho g^{1.25}}{8 {h_*}^{0.75}} \qquad \text{for shallow water}$$

The units can be cancelled out for Eq. 2 from the main text, also making its respective relationship dimensionless. Alternately, in order to express the two sides of each equation in terms of work (kilograms meters^2 seconds^{-2}), units can be selectively canceled out.

↓

$$m^2 * (kg/m^3) * (m/s^2) = m^{2.5} \times s^{0.5} \times \frac{(kg/m^3) * (m/s^2)^{1.25}}{m^{0.75}}$$

↓

$$m^2 * (kg/m^3) * (m/s^2) = m^{2.5} \times s^{0.5} \times \frac{(kg/m^3) * m^{0.5}}{s^{2.5}}$$

Cancelling and moving some terms around to make it more obviously symmetric on the two sides of the equation yields:

$$\downarrow$$

$$m^2 * (kg/m^3) * (m/s^2) \; = m^2 \; \times (kg/m^3) \; \times \; (m/s^2)$$

$$\downarrow$$

$$1 : 1$$

A deepwater version of Eq. 2 can alternately be created from Eq. 1, again using ζ = 0.5:

$$E \; \propto \left(H^2 \; \times \sqrt{\frac{H}{L}} \times \frac{L}{h_*} \right)^{0.5}$$

To do this, we similarly first square both sides, then we insert the common terms for wave energy density $\frac{1}{8}\rho g H^2$ in place of H^2, but now use the deepwater wave period $\frac{g}{2\pi}T^2$ in place of L. Next, to the left hand side, we add the bulk density of the sediment φ, and gravitational acceleration g when it moves:

$$\downarrow$$

$$E^2 \varphi g \; = \; \frac{1}{8}\rho g H^2 \times \sqrt{\frac{H}{\frac{g}{2\pi}T^2}} \times \frac{\frac{g}{2\pi}T^2}{h_*} \quad \text{for deep water}$$

$$\downarrow$$

We then offset units and move the terms around to obtain:

$$E^2 \varphi g \; = \; H^{2.5} \times \; T \times \frac{\rho g^{1.5}}{20 h_*} \quad \text{for deep water}$$

And the units can be similarly cancelled out, making its respective relationship dimensionless, or expressed in terms of work as mentioned above.

$$\downarrow$$

$$m^2 * (kg/m^3) * (m/s^2) \; = \; m^{2.5} \times s \times \frac{(kg/m^3) * (m/s^2)^{\,1.5}}{m}$$

$$\downarrow$$

Cancelling and moving some terms around to make it more obviously symmetric on the two sides of the equation yields:

$$\downarrow$$

$$m^2 * (kg/m^3) * (m/s^2) \; = m^2 \; \times (kg/m^3) \; \times \; (m/s^2)$$

1 : 1

The dimensionality, unit cancellation, and symmetry can be made far more elegant – and more obvious and easy to do - for both shallow water and deepwater relations, if instead of starting with Eq. 2 from the main text, one starts with the equation described in the subsection below entitled *Expanded Discussion*… The same basic procedure then follows of first squaring both sides, inserting the common terms for wave energy density, wave period, bulk density of the sediment and its gravitational acceleration.

Expanded Discussion: Why increasing the wave height results in greater erosion efficiency, but increasing the wavelength reduces it

The mechanics implicit in Eq. 1 appear more balanced if we square both sides, redistribute $\sqrt{H/L}$, and introduce a time duration t to both denominators:

$$\frac{E^2}{t\sqrt{H}} \propto \frac{H^2}{t\sqrt{L}} * \left(\frac{L}{h_*}\right)$$

The potential for a two-dimensional area of erosion E^2 (left hand side) is now divided by a reduced version of H in the denominator, which is to say that it is constrained along a reduced vertical dimension h_y. Similarly, the wave energy H^2 (right hand side) is constrained across a reduced horizontal dimension of the passing L. This formulation further suggests that the potential erosional area and wave energy are more-densely concentrated in specific segments of the wave form, across time.

As the wave height H independently increases, the erosional area numerator proportionally increases. However, the amount of time that the wave form intersects a discrete h_y vertical position on the edge decreases, on average, at the rate of its product with the square root of the wave height in the vertical dimension, $t\sqrt{H}$. This change in the time expended per differential unit of vertical edge occurs, because in order for a sine wave cycle to cover an increase in *H* across the entirety of L, given the same total time elapsed, the linear velocity along the sine wave must increase.

The rate of the linear velocity increase in the h dimension is directly proportional to the increase in H and is constant along the wave form, given a constant angular velocity (i.e., L is unchanged). However, the absolute magnitude of the increase along the wave form in the H dimension is inversely proportional to the distance from h_*; this is due to the nature of the sine function. In other words, the wave now spends considerably less absolute time intersecting the edge at its node h_* as compared to its crest or trough $h_{\pm y-limit}$.

If we multiply this time-spent per discrete h_y by the unchanged linear velocities in the E dimension (when L is unaltered), then the distribution of e is flattened relative to the h vertical dimension. Given constant linear and angular velocity in the horizontal dimension, the erosional face shallows in slope as H alone increases. Indeed, the rate of change in the perpendicular dimension (i.e., L), is different from that in the H (or, h) dimension, i.e., $e_y \propto 1/{h_y}^{0.25}$. The erosional shape is relative to the slope of the e distribution across H.

It follows that as the wavelength L alone independently increases (without altering H or the time duration t), the erosion decreases on a per increment of time basis at the rate of the square root of the increasing wavelength, $t\sqrt{L}$. However, the converse occurs on a per wave basis where the amount of time that the wave form intersects a discrete point of the edge increases.

The time units on either side of the above equation cancel, and so ultimately it can deliver a per wave formulation. Additionally, once H exceeds roughly double the water depth h_*, a wave breaks due to gravity. The water depth h_* can thus be seen as a modulator of the maximum realization of H^2 (i.e., H^2/h_*) or as a term in the inverse relative water depth (i.e., L/h_*). It

accounts for variation in eroding edge heights and wave height-to-water depth effects, which also greatly affect the erosion (Valentine and Mariotti 2019). Finally, as a general physical rule due to gravity and wave-breaking processes, h_* or L cannot be infinitesimally small without H being similar in magnitude.

Our description of these wave-to-erosion mechanics should be considered valid only for erosion surfaces composed of consolidated sediments. Consolidated or cohesive sediments are defined herein as those sufficient to maintain vertical and horizontal integrity against gravity or buoyant forces, as long as the peds are stacked immediately on top of one another. Non-wetland and rocky cliffs likely function similarly to wetland edges when they are under wave attack (Huppert et al. 2020). However, because these types of coastlines lie well above the water level for much longer time periods, gravity-induced mass failure and precipitation-induced erosion likely predominate (Francalanci et al. 2013) and affect the scaling of erosion.

See main text for the cited references.

Supplementary Video 1

See file Supp_video_1.MOV